bioRxiv preprint doi: https://doi.org/10.1101/2023.04.10.536237; this version posted April 12, 2023. The copyright holder for this preprint (which was not certified by peer review) is the author/funder, who has granted bioRxiv a license to display the preprint in perpetuity. It is made available under aCC-BY-ND 4.0 International license.

Palmitoylethanolamide shows limited efficacy in controlling cerebral cryptococcosis *in vivo.*

Melissa E. Munzen[1], Marta Reguera-Gomez[1], Mohamed F. Hamed[1, 2], Vanessa Enriquez[1], Claudia L. Charles-Nino[1], Michael R. Dores[3], Karina Alviña[4, 5], and Luis R. Martinez[1, 5-7*]

[1]Department of Oral Biology, University of Florida College of Dentistry, Gainesville, FL, USA; [2]Department of Pathology, Faculty of Veterinary Medicine, Mansoura University, Mansoura, Egypt; [3]Department of Biology, Hofstra University, Hempstead, NY, USA; [4]Department of Neuroscience, University of Florida, Gainesville, FL, USA; [5]Center for Translational Research in Neurodegenerative Disease, [6]Center for Immunology and Transplantation, and [7]Emerging Pathogens Institute, University of Florida, Gainesville, FL, USA.

Running Title: PEA has limited efficacy against *C. neoformans* brain infection.

Abstract: 193 words/ Text: 4,533 words/ Figures: 7/ References: 56

*To whom correspondence should be addressed:
Luis R. Martinez
University of Florida College of Dentistry
Department of Oral Biology
1395 Center Drive, DG-48
P.O. Box 100424
Gainesville, FL 32610
E-mail: LMartinez@dental.ufl.edu

CONFLICT OF INTEREST: The authors declare no conflict of interest.

bioRxiv preprint doi: https://doi.org/10.1101/2023.04.10.536237; this version posted April 12, 2023. The copyright holder for this preprint (which was not certified by peer review) is the author/funder, who has granted bioRxiv a license to display the preprint in perpetuity. It is made available under aCC-BY-ND 4.0 International license.

ABSTRACT

Cryptococcus neoformans (*Cn*) is an encapsulated neurotropic fungal pathogen and the causative agent of cryptococcal meningoencephalitis (CME) in humans. Recommended treatment for CME is Amphotericin B (AmpB) and 5-fluorocytosine (5-FC). Though effective, AmpB has displayed numerous adverse side effects due to its potency and nephrotoxicity, prompting investigation into alternative treatments. Palmitoylethanolamide (PEA) is an immunomodulatory compound capable of promoting neuroprotection and reducing inflammation. To investigate the efficacy of PEA as a therapeutic alternative for CME, we intracerebrally infected mice with *Cn* and treated them with PEA or AmpB alone or in combination. Our results demonstrate that PEA alone does not significantly prolong survival nor reduce fungal burden, but when combined with AmpB, PEA exerts an additive effect and promotes both survivability and fungal clearance. However, we compared this combination to traditional AmpB and 5-FC treatment in a survivability study and observed lower efficacy. Overall, our study revealed that PEA alone is not effective as an antifungal agent in the treatment of CME. Importantly, we describe the therapeutic capability of PEA in the context of *Cn* infection and show that its immunomodulatory properties may confer limited protection when combined with an effective fungicidal agent.

KEYWORDS: amphotericin B, *Cryptococcus neoformans*, fungal brain infection, meningoencephalitis, microglia, palmitoylethanolamide, 5-flurocytosine

bioRxiv preprint doi: https://doi.org/10.1101/2023.04.10.536237; this version posted April 12, 2023. The copyright holder for this preprint (which was not certified by peer review) is the author/funder, who has granted bioRxiv a license to display the preprint in perpetuity. It is made available under aCC-BY-ND 4.0 International license.

INTRODUCTION

Cryptococcus neoformans (*Cn*) is an encapsulated neurotropic fungal pathogen and the causative agent of cryptococcosis in humans. *Cn* causes opportunistic disease in HIV-infected individuals due to low counts of $CD4^+$ T cells, with this mycosis accounting for approximately 15 to 19% of AIDS-related deaths (1, 2). Cryptococcal meningoencephalitis (CME) is the most severe manifestation of the disease and results in an estimated 181,100 deaths annually worldwide. CME is a major cause of death in sub-Saharan Africa, where 2.5 million individuals are positive for HIV, over 58% of the global HIV-positive population (3). In fact, sub-Saharan Africa carries an estimated 73% of the global deaths related to CME annually (2). Despite the efficacy of and increasing accessibility to antifungal therapy, the high incidence of death from cryptococcal infection is associated with low adherence to antiretroviral therapy (4), as well as the lack of licensed and available treatment options (5).

The World Health Organization places cryptococcosis as a high priority mycosis and recommends a combination of amphotericin B (AmpB) and 5-flurocytosine (5-FC), followed by fluconazole as the therapeutic management of CME in severely immunosuppressed individuals (6). There are limitations to this treatment regimen, particularly with AmpB being highly toxic causing nephrotoxicity, phlebitis, hypokalaemia, and anaemia (7), often requiring hospitalization (8), and the high costs and limited accessibility of 5-FC (9). Various formulations of AmpB have been tested, such as single-dose liposomal AmpB (10), which has shown similar efficacy to conventional AmpB with fewer complications, and AmpB colloidal dispersion (11). Different combinations of antifungal therapies with AmpB have also been reviewed, such as tamoxifen (12), but fungal clearance and recovery rates have not been as effective.

bioRxiv preprint doi: https://doi.org/10.1101/2023.04.10.536237; this version posted April 12, 2023. The copyright holder for this preprint (which was not certified by peer review) is the author/funder, who has granted bioRxiv a license to display the preprint in perpetuity. It is made available under aCC-BY-ND 4.0 International license.

Palmitoylethanolamide (PEA) is an endogenous lipid compound capable of controlling and reducing neuroinflammation (13, 14). PEA downregulates the expression of inducible nitric oxide synthase and NF-κB nuclear translocation through interaction with cellular receptors, notably the peroxisome-proliferator-activated receptor alpha, present in many cell types including microglia (15). Modulation of microglial phenotypes to promote phagocytosis and migration have been observed with PEA treatment (16, 17), as well as anti-inflammatory effects, neuroprotection, reduced apoptosis, and prolonged neuronal survival (18-20). PEA enhances survival in mice infected with *Escherichia coli* by modulating inflammation and stimulating bacterial phagocytosis by microglia (21). Interestingly, PEA also acts on several molecular targets both in the central and peripheral nervous systems, making it an attractive therapeutic agent for many central nervous system-related diseases (22). In fact, a clinical trial in the 1970s in the former Czechoslovakia involving 3,600 patients demonstrated that PEA had no adverse effects at daily doses of 600 to 1,800 mg (23, 24).

The incidence of CME and limited availability of accessible, safe, and effective treatments warrant further investigation into other potential therapeutic agents. Hence, in this study, we investigated the efficacy of PEA alone or combined with other commonly used antifungal drugs (e.g., AmpB and 5-FC) during *Cn* brain infection. Using a stereotaxic model of intracerebral (i.c.) mouse infection we evaluated the potential of PEA as a candidate for the clinical management of CME.

RESULTS

AmpB and PEA combination extend the survival of C57BL/6 mice i.c.-infected with *Cn*. We first assessed the impact of PEA alone or combined with AmpB in combating cerebral

bioRxiv preprint doi: https://doi.org/10.1101/2023.04.10.536237; this version posted April 12, 2023. The copyright holder for this preprint (which was not certified by peer review) is the author/funder, who has granted bioRxiv a license to display the preprint in perpetuity. It is made available under aCC-BY-ND 4.0 International license.

cryptococcosis (Fig. 1). Using a stereotaxic apparatus (Fig. 1A), we i.c.-infected 10^4 *Cn* strain H99 cells into the mouse striatum (n = 7 mice per group, 6-8 weeks old, female), following the brain coordinates described previously (25). The striatum is a region in the basal ganglia of the brain that coordinates multiple aspects of cognition and motor function. We used it as the site of infection because this brain region is frequently affected in patients with CME (26) with cryptococcoma formation around the Virchow-Robin spaces (i.e., perivascular fluid-filled cavities that surround perforating blood vessels in the brain parenchyma) (27). One day post-infection (dpi), sterile saline (untreated), minocycline (0.5 mg/kg/d; an inhibitor of microglia activation), PEA (0.5 mg/kg/d), AmpB (3 mg/kg/d), or a combination of AmpB (3 mg/kg/d) + PEA (0.5 mg/kg/d) were administered via intraperitoneal injection (i.p.) in different groups of mice followed by every other day treatment for 28-dpi. The survivability of the untreated and treated *Cn*-infected mice was closely monitored throughout the duration of the protocol (Fig. 1B). On average but not statistically significant, PEA-treated mice that developed neurocryptococcosis survived longer (median: 13-dpi) than those in the untreated (median: 11-dpi) and minocycline-treated (median: 10-dpi) groups. Similarly, AmpB-treated animals showed much longer survival trend (median: 18-dpi) than PEA-treated mice, although this trend was not statistically significant. Interestingly, *Cn*-infected mice treated with combination of AmpB and PEA survived the longest (median: 26-dpi) with 3 out of 7 mice (approximately 42.9%) reaching to the end of the experiment (28-dpi; vs. untreated, $P < 0.001$; minocycline, $P < 0.003$; AmpB, not significant or ns; PEA, $P < 0.002$). In this regard, only one mouse in the AmpB group survived the whole experiment whereas all the untreated, minocycline-treated, and PEA-treated animals died by 15-, 24-, and 18-dpi, respectively. Clinical observations resulting from *Cn* infection included respiratory distress, neurological impairment, seizures, loss of mobility, and

bioRxiv preprint doi: https://doi.org/10.1101/2023.04.10.536237; this version posted April 12, 2023. The copyright holder for this preprint (which was not certified by peer review) is the author/funder, who has granted bioRxiv a license to display the preprint in perpetuity. It is made available under aCC-BY-ND 4.0 International license.

129 particularly, weight loss, which was a clear indicator of disease progression and mortality (Fig.
130 1C). These results indicate that while PEA alone had limited effect in extending the life of mice
131 that developed cerebral cryptococcosis, when combined with AmpB, PEA showed a
132 considerable additive effect.
133
134 **AmpB and PEA combination significantly reduces fungal burden in *Cn*-infected brains.**
135 Coronal brain tissue sections were stained with Periodic acid-Schiff to identify the morphology
136 of *Cn* in the host tissue during infection (Fig. 2). Untreated *Cn*-infected brains exhibit red-stained
137 cryptococci (arrows) in the ventricular and the caudate nucleus (Fig. 2A). Minocycline- and
138 PEA-treated brains displayed yeast cells accumulated in the margin of the cryptococcoma
139 adhering to striatal tissue. Notably, brain tissue excised from mice treated with AmpB show
140 minimal fungal colonization. *Cn*-infected mice treated with combination of PEA and AmpB
141 displayed fungal cells in the lumen of the lateral ventricle. Mice i.c.-challenged with *Cn* [$n = 6$
142 mice per group; 6 colony forming unit (CFU) plates per animal were plotted] and treated with
143 saline (untreated), minocycline, AmpB, PEA, or combination AmpB + PEA were evaluated for
144 brain fungal load (Fig. 2B). There were no differences between the groups in fungal burden at 3-
145 dpi. However, AmpB (mean: 3.72×10^6 CFU/g tissue)- and AmpB + PEA (mean: 1 CFU/g
146 tissue)-treated brains showed significantly lower fungal burden than untreated (9.14×10^6 CFU/g
147 tissue; $P < 0.0001$) or minocycline (8.04×10^6 CFU/g tissue; $P < 0.0001$)-treated brain tissue at
148 7-dpi. The AmpB + PEA combination brains exhibited the lowest CFU number reduction of all
149 the groups at the chosen dilutions. There were no differences in fungal burden between
150 untreated, minocycline-and PEA-treated mice. Overall, our findings indicate that PEA is not
151 fungicidal, although it enhances cryptococcal killing when combined with AmpB.

bioRxiv preprint doi: https://doi.org/10.1101/2023.04.10.536237; this version posted April 12, 2023. The copyright holder for this preprint (which was not certified by peer review) is the author/funder, who has granted bioRxiv a license to display the preprint in perpetuity. It is made available under aCC-BY-ND 4.0 International license.

AmpB and PEA combination stimulate strong glial cell responses around the brain region of infection. We have previously shown that *Cn* forms cryptococcomas in mouse striatal tissue after i.c. infection, mimicking CME in humans, particularly those cases with brain parenchyma involvement (28). Thus, we examined morphological changes in all saline (untreated), minocycline, AmpB, PEA, or AmpB + PEA treated *Cn*-infected mice. Brain tissue was processed for histology and sections were stained with hematoxylin & eosin, which allows us to observe tissue morphology. All treatment groups display encephalomalacia or cyptococcoma formation in the striatum (Fig. 3). Untreated brain tissue showed extensive necrosis that expanded throughout the basal ganglia (e.g., striatum, globus pallidus, and caudate nucleus; Fig. 3, top panels). Microgliosis and *Cn*-induced necrosis (red arrow) were also evident around the border of the cryptococcoma. In the minocycline-treated brains, extensive encephalomalacia that extended to the overlying cerebral cortex was observed (Fig 3, second panel row from the top). In addition, *Cn* invaded the tissue surrounding the cryptococcoma causing ischemic neuronal necrosis (blue arrow) and weak microglial response (red arrow), which is characteristic of GXM accumulation and the direct negative effect of minocycline in these glial cells (25). Interestingly, tissue from AmpB-treated mice evinced marked microgliosis (blue arrow) and astrocytic response (red arrow) in tissue adjacent to the cryptococcoma or encephalomalacia (middle row panels), while tissue from PEA-treated mice displayed noticeable microgliosis (red arrow) and evident swollen endothelial cells (blue arrow). Lastly, *Cn*-infected mice and treated with combination of AmpB + PEA exhibited microgliosis (red arrow) around the margin of the cryptococcoma (Fig. 3, lower panels). In summary, analysis of our histological data demonstrate

bioRxiv preprint doi: https://doi.org/10.1101/2023.04.10.536237; this version posted April 12, 2023. The copyright holder for this preprint (which was not certified by peer review) is the author/funder, who has granted bioRxiv a license to display the preprint in perpetuity. It is made available under aCC-BY-ND 4.0 International license.

that AmpB + PEA stimulate robust glial cell responses that may be critical to combat *Cn* brain infection.

AmpB and PEA combination reduces *Cn* GXM released in brain tissue. *Cn* GXM is abundantly secreted during infection resulting in immunosuppressive effects for the host. Hence, we examined the impact of these various drug treatments on GXM accumulation in tissue during cerebral cryptococcosis (Fig. 4). GXM was red-pink stained in brain tissue using the specific monoclonal antibody (mAb) 18B7 (Fig. 4A). The GXM intensity in tissue sections was analyzed using NIH Image J color deconvolution tool software. Immunolabeling of untreated *Cn*-infected brain tissue evinced extensive GXM accumulation that diffused inside the lateral ventricle. Minocycline-injected animals displayed GXM concentrated in the area of encephalomalacia that spread to surrounding brain tissue. In contrast, *Cn*-infected brains from PEA treated mice showed localized polysaccharide accumulation inside the cryptococcoma without dissemination to surrounding tissue (Fig. 4A, middle panels). Interestingly, AmpB-treated groups (either alone or in combination with PEA) demonstrated a significant reduction in GXM accumulation in brain tissue (Fig. 4A and B). Further, brains from mice treated with AmpB + PEA combination showed positive immunostaining exclusively in plug-like structures (arrow) formed and adhered to ependymal cells in the lateral ventricle, without brain parenchyma involvement (Fig. 4A, lower panels). Analysis of the intensity of GXM staining in brain tissue images from *Cn*-infected mice after the various drug treatments revealed that AmpB alone and in combination with PEA had significantly lower GXM intensity or accumulation in tissues than minocycline- ($P < 0.05$) and PEA-treated ($P < 0.01$) groups (Fig. 4B). Our data show that AmpB regulates fungal

bioRxiv preprint doi: https://doi.org/10.1101/2023.04.10.536237; this version posted April 12, 2023. The copyright holder for this preprint (which was not certified by peer review) is the author/funder, who has granted bioRxiv a license to display the preprint in perpetuity. It is made available under aCC-BY-ND 4.0 International license.

196 capsular polysaccharide release, which may have important implications for impacting the
197 progression of neurocryptococcosis.
198
199 **PEA has no effect in reducing *Cn* capsular volume *in vivo.*** The capsule of *Cn* is the primary
200 virulence factor of the fungus and is incredibly dynamic and responsive to changes in the
201 microenvironment. Large capsule volume is correlated with a robust inflammatory response and
202 respiratory distress (29). Also, capsular enlargement reduces phagocytosis and enhances *Cn*
203 survival during infection (30). To validate our results indicating that AmpB treatment reduces *Cn*
204 GXM released in brain tissue, we assessed the impact of the different drug treatments on
205 capsular size and volume in brain tissue homogenates using India ink staining and light
206 microscopy (Fig. 5A). Quantification of microscopic images (n = 3 mice and ≥ 200 cells per
207 group; Fig. 5B) confirmed that treatment with AmpB (1,208.2 μm^3; $P < 0.05$) and AmpB + PEA
208 (1,259.9 μm^3; $P < 0.05$) significantly reduced *Cn* capsular volume compared to minocycline
209 treatment (1,643.2 μm^3). Surprisingly, no differences in capsular volume were observed between
210 untreated (1,394.6 μm^3), PEA (1,350.1 μm^3), AmpB (1,208.2 μm^3), and AmpB + PEA (1,259.9
211 μm^3). Our results suggest that AmpB, on average, has a negative effect on cryptococcal capsular
212 production and release in brain tissue, thus, facilitating fungal clearance during infection.
213
214 **PEA causes similar microglia morphological changes than minocycline during *Cn* brain**
215 **infection.** Microglia are the principal immune cell in the brain responsible for phagocytosis,
216 immune cell recruitment, and communication via cytokine signaling (31). We recently reported
217 that microglia can take diverse morphological phenotypes after *Cn* i.c.-infection, ramified,
218 activated, phagocytic/amoeboid, dystrophic, or rod-shaped, which may be associated with

bioRxiv preprint doi: https://doi.org/10.1101/2023.04.10.536237; this version posted April 12, 2023. The copyright holder for this preprint (which was not certified by peer review) is the author/funder, who has granted bioRxiv a license to display the preprint in perpetuity. It is made available under aCC-BY-ND 4.0 International license.

219 neurocryptococcosis progression and outcome (28). Therefore, we monitored the impact of each
220 drug treatment on the phenotypic landscape of microglia during cryptococcal infection (Fig. 6).
221 Microglia and GXM were immunolabeled using ionized calcium binding adaptor molecule-1
222 (Iba-1; brown)- and 18B7 (pink-red)-binding mAbs, respectively (Fig. 6A). Images of each
223 group treatment were visualized under the microscope and the microglia morphology
224 documented as previously described (25). *Cn*-infected brains from untreated mice presented the
225 following microglia phenotype distribution: activated (38.52%) > ramified (31.03%) > rod-
226 shaped (15.46%) > phagocytic (11.59%) > dystrophic (3.4%) (Fig. 6B). Although minocycline
227 treatment inhibited microglial activation (32.46%), this drug resulted in the highest percentage of
228 phagocytic (42.8%) and dystrophic (9.58%) microglia and the lowest percentage of ramified
229 (6.03%) microglia. In addition, brains from minocycline-treated mice had the second lowest
230 percentage of rod-shaped (9.12%) microglia after AmpB-treated (8.46%) mice. Furthermore,
231 AmpB-treatment resulted in the highest percentage of ramified (44.58%) microglia and the
232 lowest percentage of activated (22.78%) microglia. Tissue from AmpB-treated mice also had
233 20.93% and 3.25% of phagocytic and dystrophic microglia, respectively. The phenotypic profile
234 of microglia in PEA-treated tissue was similar to those observed in the minocycline group
235 including 39.32% phagocytic, 35.77% activated, 11.69% rod-shaped, 10.37% ramified, and
236 2.85% dystrophic morphology. Moreover, AmpB + PEA-treated animals evinced similar
237 microglia morphological patterns than untreated mice including 32.48% activated, 30.18%
238 ramified, 14.86% rod-shaped, 20.18% phagocytic, and 2.29% dystrophic cells. Our findings
239 suggest that *Cn* brain infection and different drug treatments causes phenotypic microglial
240 alterations, which may have important consequences in their responses to fungal infection and
241 clearance.

bioRxiv preprint doi: https://doi.org/10.1101/2023.04.10.536237; this version posted April 12, 2023. The copyright holder for this preprint (which was not certified by peer review) is the author/funder, who has granted bioRxiv a license to display the preprint in perpetuity. It is made available under aCC-BY-ND 4.0 International license.

PEA and AmpB combination prolong i.c.-infected mouse survival, but with less efficacy to current standard of treatment. Since AmpB and 5-FC are standard of treatment for individuals with CME, we compared the efficacy of PEA and AmpB combination and AmpB and 5-FC combination in extending *Cn*-infected mice survival (Fig. 7). On average, *Cn*-infected and AmpB + PEA-treated mice exhibited higher survivability (median: 20-dpi) relative to untreated (median: 12-dpi; $P < 0.03$) and PEA + 5-FC (median: 14-dpi; trend but ns) animals (Fig. 7A). All untreated mice and PEA + 5-FC-treated groups died by 20-dpi. On the contrary, all mice infected with *Cn* and treated with AmpB + 5-FC survived (100%; vs. Untreated, $P < 0.001$; PEA + 5-FC, $P < 0.001$) whereas only 33% (2 out of 6) of the animals in the AmpB + PEA group ($P < 0.02$) survived for 28-dpi when the experiment was finalized. Body weight was monitored and was also a clear indicator of disease progression, with mortality being associated with 25% weight loss (Fig. 7B). These results show that while the combination of AmpB and PEA has positive effects in prolonging the life of mice with cerebral cryptococcosis, this effect is limited when compared with the efficacy of AmpB and 5-FC, the current standard of patient care.

DISCUSSION

In this study, we demonstrated that PEA has limited effect in prolonging murine survivability upon direct brain infection with *Cn*. PEA is an immunomodulatory molecule, and its effects in extending mouse survival are related to the high activation of microglia in brain tissue that may aid in combating *Cn* infection. Our data show that 75% of microglia during *Cn* brain infection had an activated or phagocytic phenotype, which is critical for microbial clearance (32). For example, PEA increases microglia-mediated phagocytosis of bacteria without

bioRxiv preprint doi: https://doi.org/10.1101/2023.04.10.536237; this version posted April 12, 2023. The copyright holder for this preprint (which was not certified by peer review) is the author/funder, who has granted bioRxiv a license to display the preprint in perpetuity. It is made available under aCC-BY-ND 4.0 International license.

inducing considerable inflammation (33), prevents rheumatic fever in susceptible children (34), and alters the course of influenza infection (24). However, its limitation in controlling *Cn* infection is because PEA has no direct effect in killing the fungus, reducing cryptococcoma formation, or decreasing fungal capsular volume and GXM secretion. Interestingly, PEA provides a substantial additive effect in combating cerebral cryptococcosis when combined with AmpB, which although toxic to the host, is a potent anti-cryptococcal agent, validating the critical importance of antimicrobial compounds in stimulating the host immunity. Combination of AmpB and PEA significantly and surprisingly decreased CFU numbers in *Cn* brain infected mice relative to all the other tested groups. Despite cryptococcoma formation in brain tissue of animals treated with AmpB and PEA combination, histopathology shows considerable microgliosis surrounding the brain-lesions, which is consistent with fungal clearance. Although i.c. infected mice treated with either AmpB or PEA elicited a strong glial response, it is plausible to consider that the AmpB and PEA combination provides an ideal balance between the potency of the antifungal drug and the lipid in killing the fungus. It is possible that PEA, by being a hydrophobic molecule, binds to the cell membrane ergosterol and serves as a vehicle in facilitating AmpB-mediated pore formation, killing the cell (35). These hypotheses are possible given that untreated and minocycline-treated brains showed moderate to weak glial responses and the untreated tissue exhibited ischemic necrosis, a manifestation reported in patients with CME (36, 37) and in this model of infection (25).

Untreated and minocycline- or PEA-treated *Cn* infected brains exhibited extensive accumulation of GXM in tissue. Additionally, cryptococci isolated from the brains of these groups showed large capsule size and volume relative to the AmpB-treated groups of animals. Enlargement of the capsule reduces phagocytosis during infection and dramatically enhances

bioRxiv preprint doi: https://doi.org/10.1101/2023.04.10.536237; this version posted April 12, 2023. The copyright holder for this preprint (which was not certified by peer review) is the author/funder, who has granted bioRxiv a license to display the preprint in perpetuity. It is made available under aCC-BY-ND 4.0 International license.

288 virulence through oxidative stress resistance (30, 38). However, cryptococcal GXM
289 accumulation showed different patterns with untreated and minocycline-treated tissue displaying
290 polysaccharide intensity throughout tissue surrounding the cryptococcoma, whereas PEA-treated
291 tissue exhibited higher GXM intensity inside of cryptococcomas or region of encephalomalacia.
292 It is conceivable that differential glial cell responses (e.g., microglia and astrocytes) between
293 these groups modulate the extension (e.g., untreated and minocycline) of GXM secretion from or
294 containment (e.g., PEA) within the cryptococcoma. This is important because GXM inhibits T
295 cell proliferation and reduces leukocyte recruitment needed for fungal clearance (39). Notably,
296 AmpB and AmpB + PEA brains infected with the fungus evinced little or localized tissue
297 secretion of GXM, respectively, which is likely due to the smaller capsular volume shown by the
298 cryptococci and reduction in proliferation or killing of the fungi. AmpB reduces capsule size and
299 serum polysaccharide, a described mechanism for this antifungal drug efficacy in cryptococcosis
300 (40). Regardless of its high toxicity, AmpB has been used for the treatment of disseminated
301 cryptococcal disease for over 70 years (41), and novel anti-cryptococcal compounds causing
302 minimal toxicity are urgently needed.

303 Microglia are dynamic resident immune cells of the central nervous system that can
304 modify their phenotype based on their responses to various pathological insults (42). Microglia
305 engulf cryptococci, which can survive and replicate inside these cells (43), avoiding immune
306 recognition. The morphological distribution of microglia in brain tissue after *Cn* brain infection
307 and the various treatments differed among the groups and may have important predictor
308 implications in reducing mortality. For instance, untreated *Cn*-infected brains showed the highest
309 and lowest percentages of rod-shaped and phagocytic morphologies by microglia, respectively.
310 Descriptions of rod-shaped microglia, which present elongated nuclei, few processes, and are

bioRxiv preprint doi: https://doi.org/10.1101/2023.04.10.536237; this version posted April 12, 2023. The copyright holder for this preprint (which was not certified by peer review) is the author/funder, who has granted bioRxiv a license to display the preprint in perpetuity. It is made available under aCC-BY-ND 4.0 International license.

most notable in chronic neurological disorders, are scarce. The function of these cells remains under investigation, but it is believed that they may provide neuroprotection and trophic support (44, 45). Hypertrophic microglia are thought to be actively responding to injury (46, 47) and were most abundant in untreated *Cn*-infected brains mostly due to tissue destruction related to encephalomalacia. Hypertrophic microglial densities are directly related to cortical atrophy in Alzheimer's disease and inversely related to high density of functional neurons in tissue (48). Thus, accumulation of activated microglia may occur in damaged blood vessels or microinfarctions during cryptococcal infection. It is also possible that GXM accumulation makes activated microglia anergic or unresponsive, thus, the low phagocytic or amoeboid morphology displayed, which may facilitate the proliferation and survival of the fungus, enhancing the progression of the cerebral disease. Both minocycline- and PEA-treated tissues presented approximately three quarters of all microglial cells activated and phagocytic, but animals in both groups have low number of ramified microglia. Activated or hypertrophic microglia has been linked to oxidative stress and inflammation in neurological diseases such Alzheimer's (49), Parkinson's (50), stroke (51), and others. Moreover, minocycline-treated animals exhibited the highest number of dystrophic microglia, which have fragmented processes, probably due to cell dysfunction. Dystrophic microglia are found in high numbers in vulnerable individuals who suffer from brain degeneration (52, 53) or senescence (44) due to aging or neurological diseases. Interestingly, brains excised from AmpB and combination of AmpB and PEA groups showed similarly balanced activated, phagocytic, ramified microglia distribution percentages. It is conceivable that the highest number of ramified and rod-shaped microglia present in AmpB- and combination-treated animals, respectively, makes a difference in the fungal persistence or clearance observed in these groups, possibilities that can be tested in future studies. Elucidating

bioRxiv preprint doi: https://doi.org/10.1101/2023.04.10.536237; this version posted April 12, 2023. The copyright holder for this preprint (which was not certified by peer review) is the author/funder, who has granted bioRxiv a license to display the preprint in perpetuity. It is made available under aCC-BY-ND 4.0 International license.

334 the impact of microglial responses or phenotypes in brain tissue infected with *Cn* is necessary
335 given their central role in many neurodegenerative diseases, including CME, which leads to
336 cognitive decline and mortality in patients (54).

337 Treatment of *Cn*-infected mice with combination of AmpB + PEA revealed less efficacy
338 than the recommended standard combination of AmpB + 5-FC. All the mice treated with the
339 standard of care combination survived through the duration (28-dpi) of the experiment. However,
340 mortality associated with CME in humans even with optimal treatment remains high (55).
341 Therefore, novel treatments that rapidly improve the clinical manifestation associated with CME
342 such as intracranial pressure and high fungal burden in the cerebrospinal fluid. Here, we
343 demonstrated that PEA is not an effective antifungal drug but may be beneficial in modulating
344 the immune response in combination with an effective fungicidal drug. Further pre-clinical
345 studies investigating the efficacy of immunomodulator molecules for the treatment of CME
346 could provide medical professionals with additional cost-effective and safe antifungal therapy
347 options of care especially in developing countries.

348

349 **MATERIALS AND METHODS**

350 **Ethics statement.** All animal studies were conducted according to the experimental practices
351 and standards approved by the Institutional Animal Care and Use Committee (IACUC) at the
352 University of Florida (Protocol #: 202011067). The IACUC at the University of Florida
353 approved this study.

354

bioRxiv preprint doi: https://doi.org/10.1101/2023.04.10.536237; this version posted April 12, 2023. The copyright holder for this preprint (which was not certified by peer review) is the author/funder, who has granted bioRxiv a license to display the preprint in perpetuity. It is made available under aCC-BY-ND 4.0 International license.

355 ***Cn.*** *Cn* strain H99 (serotype A) was isolated and kindly provided by John Perfect at Duke
356 University. Yeasts were grown in Sabouraud dextrose broth (pH 5.6; BD Difco) for 24 h at 30°C
357 in an orbital shaker (Thermo Fisher) set at 150 rpm (to early stationary phase).
358
359 **i.c. infection with *Cn*.** C57BL/6 female mice (6-8 weeks old; Envigo) were anesthetized using
360 isoflurane (3–5% for induction and 1–2% maintenance; model: VetFlo Vaporizer Single Channel
361 Anesthesia System, Kent Scientific), placed in prone position over a heating pad (model:
362 RightTemp Jr., Kent Scientific), and prepped using standard aseptic techniques. A local
363 anesthetic, bupivacaine or ropivacaine (0.05%; Covetrus), was administered subcutaneously in
364 the incision. The fur on the skull was carefully shaved off and the animal was securely placed in
365 a stereotaxic apparatus (model: 940; Kopf Instruments).
366 Using a small hand-held microdrill (model: Ideal microdrill; Braintree Scientific), the
367 skull was thinned until the underlying dura mater was visible and a 26 G Hamilton syringe was
368 brought to the correct stereotaxic position and lowered until it touched the exposed dura. The
369 craniotomy was around 1 mm in diameter and the correct brain coordinates were identified using
370 a stereotaxic brain atlas (e.g., The Allen Mouse Brain Atlas; https://mouse.brain-
371 map.org/static/atlas). Based on our recent study (25) and others (56, 57) using the *Cn* H99 strain,
372 a 1-µL suspension containing 10^4 cryptococci in sterile saline was injected into the striatum
373 [Stereotaxic coordinates: x (medial/lateral), -2; y (anterior/posterior), 0.2; z (dorsal/ventral), -
374 3.5)] using a 26 G Hamilton syringe connected to a pump (model: UltraMicroPump3; World
375 Precision Instruments). We injected the fungal inoculum in a 1-µL volume to avoid tissue
376 damage or diffusion of the cryptococci to other regions of the brain. The skin incision on the

bioRxiv preprint doi: https://doi.org/10.1101/2023.04.10.536237; this version posted April 12, 2023. The copyright holder for this preprint (which was not certified by peer review) is the author/funder, who has granted bioRxiv a license to display the preprint in perpetuity. It is made available under aCC-BY-ND 4.0 International license.

dorsal head was closed with sterile nylon suture and 2-4% topical chlorhexidine solution was be applied over the closed incision. After the surgery, mice were placed on a clean recovery cage.

Administration of drug treatments. One-dpi, mice were injected with a 100 µL solution of sterile saline, minocycline (0.5 mg/kg/day (d); diluted in sterile saline; ACROS Organics), AmpB (3 mg/kg/d; diluted in sterile saline; AmpB; Gibco), PEA (0.5 mg/kg/d; diluted in sterile saline; Tokyo Chemical Industry), or AmpB (3 mg/kg/d) + PEA (0.5 mg/kg/d) combination i.p. every other day and monitored for survivability. In separate infections, mice were euthanized at determined time points via CO_2 inhalation and brain tissues were excised for processing for determination of CFU numbers and histopathological studies. Similarly, 5-fluorocytosine (100 mg/kg/d; diluted in sterile saline; 5-FC; ThermoFisher) was used in combination with PEA (0.5 mg/kg/d) or AmpB (3 mg/kg/d) and survivability was determined. The survival end points were inactivity, tachypnea, or loss of ≥ 25% of body weight from baseline weight. We monitored the mice twice daily for clinical signs, dehydration, and weight loss. Animals showing signs of dehydration or that lost more than 10% weight received supportive care such as 1 mL of parenteral fluid supplementation (saline) and moist chow on the cage floor was provided.

CFU determinations. Brains were excised from euthanized mice and weighed 3- and 7-dpi. The brain tissue was homogenized in 5 mL of sterile phosphate buffered saline, serially diluted, a 100 µL suspension was plated on Sabouraud dextrose agar (BD Difco) and incubated at 30°C for 48 h. Quantification of viable yeast cells from infected animals were determined by CFU counting of two dilutions per animal (n = 6 per day).

bioRxiv preprint doi: https://doi.org/10.1101/2023.04.10.536237; this version posted April 12, 2023. The copyright holder for this preprint (which was not certified by peer review) is the author/funder, who has granted bioRxiv a license to display the preprint in perpetuity. It is made available under aCC-BY-ND 4.0 International license.

Brain histology. The brains were harvested and immersed in 4% paraformaldehyde (Fisher) overnight. Then, brains were washed 3X with sterile saline for 1 h, embedded in paraffin, 4 µm coronal sections were serially cut using a cryostat (Tanner Scientific, model: TN50), fixed onto glass slides, and subjected to hematoxylin & eosin or Periodic acid-Schiff staining to examine tissue or fungal morphology, respectively. GXM (MAb 18B7 is an anti-cryptococcal GXM IgG1 generated and generously provided by Arturo Casadevall at the Johns Hopkins Bloomberg School of Public Health; 1:1,000 dilution) and Iba-1 (rabbit anti-human Iba-1; 1:1,000 dilution; FujiFilm Wako) specific Ab (conjugated to horseradish peroxidase; dilution: 1:1,000; Santa Cruz Biotechnology) immunostaining to assess capsular release and distribution and microglial phenotype, respectively, near cryptococcomas. The slides were visualized using a Leica DMi8 inverted microscope, and images were captured with a Leica DFC7000 digital camera using LAS X digital imaging software. GXM distribution in tissue sections at 10X magnification (n = 15 fields per brain) was calculated using NIH Image J color deconvolution tool software (version 1.53q). The mean color intensity of the GXM for each treatment group was plotted in Prism version 9.5 (GraphPad). The images were examined and analyzed by Dr. Mohamed F. Hamed, a veterinary pathologist.

Capsule measurements with India ink. The capsules of cryptococci present in the brain tissue of infected mice were measured from 10-µL of homogenates prepared in phosphate-buffered saline. India ink stain (BD Scientific) was diluted 1:5 in sterile milli-Q water and used to visualize the capsules under light microscopy. Images were taken with a Leica DMi8 inverted microscope and DFC7000 T digital camera. The diameters of both capsule and cell body were measured using the Leica software platform LAS X. Capsule volume was calculated for ≥ 200

bioRxiv preprint doi: https://doi.org/10.1101/2023.04.10.536237; this version posted April 12, 2023. The copyright holder for this preprint (which was not certified by peer review) is the author/funder, who has granted bioRxiv a license to display the preprint in perpetuity. It is made available under aCC-BY-ND 4.0 International license.

cells per group (n = 3 animal per group) using the volume formula, where R = radius of capsule and r = radius of cell body: capsule volume (V) = 4/3 $\pi(R^2-r^2)$.

Statistical analysis. All data were subjected to statistical analysis using Prism 9.5 (GraphPad). Differences in survival rates were analyzed by the log-rank test (Mantel-Cox). *P* values for multiple comparisons were calculated by one-way analysis of variance (ANOVA) and were adjusted by use of the Tukey's *post-hoc* analysis. *P* values of <0.05 were considered significant.

FIGURE LEGENDS

Fig. 1. Palmitoylethanolamide (PEA) treatment prolongs survival of C57BL/6 mice infected with *C. neoformans* (*Cn*) when combined with Amphotericin B (AmpB). (A) Experimental timeline for the intracerebral (i.c.) *Cn* infection and every other day intraperitoneal (i.p.) treatment model used in this study. Mice (n=7 animals per group) were infected with 10^4 *Cn* strain H99 and administered treatments (e.g., saline (untreated), minocycline, AmpB, PEA, and AmpB + PEA) by i.p. injection every other day. Then, survival studies and colony forming units (CFU) determinations, histopathology, and microscopy were performed 3- and 7-days post-infection (dpi). The diagram was created with BioRender.com by Melissa E. Munzen. **(B)** Survival differences of C57BL/6 mice i.c. infected. Significance ($P < 0.05$) was calculated by log-rank (Mantel-Cox) analysis. *, #, and X indicate statistically different than untreated, minocycline-, and PEA-treatment groups, respectively. **(C)** Body weight was monitored for changes and development of clinical symptoms indicative of mice nearing endpoint. Each time point corresponds to mean weight and error bars denote standard deviations (SDs).

bioRxiv preprint doi: https://doi.org/10.1101/2023.04.10.536237; this version posted April 12, 2023. The copyright holder for this preprint (which was not certified by peer review) is the author/funder, who has granted bioRxiv a license to display the preprint in perpetuity. It is made available under aCC-BY-ND 4.0 International license.

Fig. 2. PEA and AmpB combination reduces cryptococcal burden in brains of mice 7 days post-infection (dpi). (A) Periodic acid-Schiff-stained 4 μm brain sections indicating infection by *Cn* in C57BL/6 mice (n = 3 mice per group). Mouse brains were excised 7-dpi. Representative 10X (left panel), 20X (left center panel), 40X (right center panel), and 100X (right panel) magnifications (red-stained *Cn* cell wall; scale bar: 50 μm) are shown. Panel images are a magnification of the black rectangle in the corresponding left-stained section to display tissue morphology surrounding cryptococcoma in each treatment group. Arrows indicate cryptococci. **(B)** Fungal burden (CFU) in brains collected from *Cn* H99-infected mice (n = 6 mice per group) at 3- and 7-dpi. Quantification of viable yeast cells from infected animals were determined by CFU counting from two dilutions per mouse (n = 6 plates per animal) in phosphate-buffered saline (PBS). CFU determinations are based on detectable colonies at the defined concentrations in PBS (for 3-dpi, 1:1,000 and 1:10,000; for 7-dpi, 1: 10,000 and 1:50,000). Each symbol represents a single CFU determination (n = 36 plates per group). Bars and error bars denote means and SDs, respectively. Significance (****, $P < 0.0001$; ***, $P < 0.001$) was calculated by one-way analysis of variance (ANOVA) and adjusted using Tukey's *post hoc* analysis. ns denotes comparisons which are not statistically significant.

Fig. 3. Robust glial cell responses were observed around the brain region of infection of mice treated with AmpB and PEA combination. Hematoxylin & eosin (7-dpi)-stained brain sections (4 μm thickness) from i.c. infected mice with *Cn* H99 (n = 3 per group) and treated with saline (untreated), minocycline, AmpB, PEA, or AmpB + PEA. Representative 10X (left panel), 20X (left center panel), 40X (right center panel), and 100X (right panel) magnifications images

bioRxiv preprint doi: https://doi.org/10.1101/2023.04.10.536237; this version posted April 12, 2023. The copyright holder for this preprint (which was not certified by peer review) is the author/funder, who has granted bioRxiv a license to display the preprint in perpetuity. It is made available under aCC-BY-ND 4.0 International license.

468 are shown. Arrows indicate histological changes described in the result section text. Scale bars:
469 50 μm.
470
471 **Fig. 4. C57BL/6 mice treated with AmpB or AmpB + PEA showed significant reduction in**
472 ***Cn* glucuronoxylomannan (GXM) secretion. (A)** Representative images of brain tissue
473 sections (7-dpi) from *Cn* H99-infected mice treated with saline (untreated), minocycline, AmpB,
474 PEA, or AmpB + PEA co-stained with GXM-specific monoclonal antibody (mAb 18B7; red-
475 pink) and ionized calcium binding adaptor molecule-1 (Iba-1; brown) marker for microglia.
476 Representative 10X (left panel), 20X (left center panel), 40X (right center panel), and 100X
477 (right panel) magnifications are shown. Panel images are a magnification of the black rectangle
478 in the corresponding left-stained section to display tissue morphology surrounding
479 cryptococcoma in each treatment group. Arrow indicates plugs adhered to the ependymal cells.
480 Scale bars: 50 μm. **(B)** Quantification of GXM intensity. Regions of GXM release were
481 measured (n = 15 fields per group). Boxes and whiskers denote means and SDs, respectively.
482 Significance (**, $P < 0.01$; *, $P < 0.05$) was calculated by one-way ANOVA and adjusted using
483 Tukey's *post hoc* analysis. ns denotes comparisons which are not statistically significant.
484
485 **Fig. 5. Brains from C57BL/6 mice treated with AmpB or AmpB + PEA exhibit cryptococci**
486 **with considerable capsule size decrease. (A)** Images of brain homogenates (7-dpi) from mice
487 i.c. infected with 10^4 *Cn* cells and treated with saline (untreated), minocycline, AmpB, PEA, or
488 AmpB + PEA. Fungal cells were stained with India Ink. Each image was examined by light
489 microscopy using a Leica DMi8 inverted microscope and images captured with a Leica
490 DFC7000 digital camera using LAS X digital imaging software. **(B)** Capsule volume (V = 4/3

bioRxiv preprint doi: https://doi.org/10.1101/2023.04.10.536237; this version posted April 12, 2023. The copyright holder for this preprint (which was not certified by peer review) is the author/funder, who has granted bioRxiv a license to display the preprint in perpetuity. It is made available under aCC-BY-ND 4.0 International license.

491 $\pi(R^2-r^2)$ for *Cn* cells in brain homogenates from each group was calculated using Leica LAS X
492 software. Brain homogenates from 3 mice per group were analyzed, and ≥ 200 cells were
493 measured. Bars and error bars denote means and SDs, respectively. Significance (*, $P < 0.05$)
494 was calculated by one-way ANOVA and adjusted using Tukey's *post hoc* analysis. ns denotes
495 comparisons which are not statistically significant.
496
497 **Fig. 6. Differential microglial morphology in brain tissue infected with *Cn* after treatment**
498 **with AmpB, PEA, or combination. (A)** Representative images of brain tissue sections (7-dpi)
499 from *Cn* H99-infected mice (n = 3 mice per group) treated with saline (untreated), minocycline,
500 AmpB, PEA, or AmpB + PEA co-stained with mAb 18B7 (GXM, red-pink) and Iba-1
501 (microglia, brown). Representative 10X (left panel), 20X (left center panel), 40X (right center
502 panel), and 100X (right panel) magnifications are shown. Panel images are a magnification of the
503 black rectangle in the corresponding left-stained section to display microglia morphological
504 changes near a cryptococcoma in each treatment group. Scale bars: 50 μm. **(B)** Pie charts
505 showing the percentage of microglial morphology distribution (e.g., activated, ramified,
506 dystrophic, phagocytic/amoeboid, and rod-shaped cells) in brain tissue during infection with *Cn*
507 H99 and different treatments. Microglial phenotype abundance was visualized using light
508 microscopy and classified according to their morphology.
509
510 **Fig. 7. Combination of AmpB and PEA prolongs survival of C57BL/6 mice, although not**
511 **with efficacy comparable to AmpB and 5-Fluorocytosine (5-FC). (A)** Survival differences of
512 C57BL/6 mice i.c. infected with 10^4 *Cn* strain H99 (n = 6 per group) and every other day given
513 i.p. treatment with saline (untreated), AmpB + PEA, PEA + 5-FC, or AmpB + 5-FC.

bioRxiv preprint doi: https://doi.org/10.1101/2023.04.10.536237; this version posted April 12, 2023. The copyright holder for this preprint (which was not certified by peer review) is the author/funder, who has granted bioRxiv a license to display the preprint in perpetuity. It is made available under aCC-BY-ND 4.0 International license.

514 Significance ($P < 0.05$) was calculated by log-rank (Mantel-Cox) analysis. *, #, and X indicate
515 statistically different than untreated, AmpB + PEA-, and PEA + 5-FC-treatment groups,
516 respectively. **(B)** Body weight was monitored for changes and development of clinical symptoms
517 indicative of mice nearing endpoint. Each time point corresponds to mean weight and error bars
518 denote SDs.
519
520 **ACKNOWLEDGEMENTS**
521 M.E.M., M.R-G, M.F.H., C.L.C-N, M.R.D., and L.R.M. were supported by the National Institute
522 of Allergy and Infectious Diseases (NIAID award # R01AI145559) of the US National Institutes
523 of Health (NIH). V.E. was supported by the UFCD's Comprehensive Training Program in Oral
524 Biology (NIH NIDCR Award # T90DE021990/R90DE022530). K.A. was funded by The Florida
525 Department of Health Ed and Ethel Moore Alzheimer's Disease Research Program (Award #
526 21A12). The funders had no role in the study design, data collection and analysis, decision to
527 publish, or preparation of the manuscript.
528
529 **AUTHORSHIP CONTRIBUTIONS**
530 All authors contributed to the project design and experimental procedures, analyzed data,
531 provided the figure presentation, and manuscript writing.
532
533 **REFERENCES**
534 1. Kabir Z, Cunningham C. 2022. The global burden of cryptococcosis-a neglected tropical
535 disease? Lancet Infect Dis 22:1658-1660.
536 2. Rajasingham R, Smith RM, Park BJ, Jarvis JN, Govender NP, Chiller TM, Denning DW,
537 Loyse A, Boulware DR. 2017. Global burden of disease of HIV-associated cryptococcal
538 meningitis: an updated analysis. Lancet Infect Dis 17:873-881.

bioRxiv preprint doi: https://doi.org/10.1101/2023.04.10.536237; this version posted April 12, 2023. The copyright holder for this preprint (which was not certified by peer review) is the author/funder, who has granted bioRxiv a license to display the preprint in perpetuity. It is made available under aCC-BY-ND 4.0 International license.

3. Rajasingham R, Govender NP, Jordan A, Loyse A, Shroufi A, Denning DW, Meya DB, Chiller TM, Boulware DR. 2022. The global burden of HIV-associated cryptococcal infection in adults in 2020: a modelling analysis. Lancet Infect Dis 22:1748-1755.
4. Williamson PR, Jarvis JN, Panackal AA, Fisher MC, Molloy SF, Loyse A, Harrison TS. 2017. Cryptococcal meningitis: epidemiology, immunology, diagnosis and therapy. Nat Rev Neurol 13:13-24.
5. Kneale M, Bartholomew JS, Davies E, Denning DW. 2016. Global access to antifungal therapy and its variable cost. J Antimicrob Chemother 71:3599-3606.
6. Perfect JR, Dismukes WE, Dromer F, Goldman DL, Graybill JR, Hamill RJ, Harrison TS, Larsen RA, Lortholary O, Nguyen MH, Pappas PG, Powderly WG, Singh N, Sobel JD, Sorrell TC. 2010. Clinical practice guidelines for the management of cryptococcal disease: 2010 update by the infectious diseases society of america. Clin Infect Dis 50:291-322.
7. Warrell CE, Macrae C, McLean ARD, Wilkins E, Ashley EA, Smithuis F, Tun NN. 2021. Ambulatory induction phase treatment of cryptococcal meningitis in HIV integrated primary care clinics, Yangon, Myanmar. BMC Infect Dis 21:375.
8. Meiring S, Fortuin-de Smidt M, Kularatne R, Dawood H, Govender NP, Germs SA. 2016. Prevalence and Hospital Management of Amphotericin B Deoxycholate-Related Toxicities during Treatment of HIV-Associated Cryptococcal Meningitis in South Africa. PLoS Negl Trop Dis 10:e0004865.
9. Rajasingham R, Rolfes MA, Birkenkamp KE, Meya DB, Boulware DR. 2012. Cryptococcal meningitis treatment strategies in resource-limited settings: a cost-effectiveness analysis. PLoS Med 9:e1001316.
10. Jarvis JN, Lawrence DS, Meya DB, Kagimu E, Kasibante J, Mpoza E, Rutakingirwa MK, Ssebambulidde K, Tugume L, Rhein J, Boulware DR, Mwandumba HC, Moyo M, Mzinganjira H, Kanyama C, Hosseinipour MC, Chawinga C, Meintjes G, Schutz C, Comins K, Singh A, Muzoora C, Jjunju S, Nuwagira E, Mosepele M, Leeme T, Siamisang K, Ndhlovu CE, Hlupeni A, Mutata C, van Widenfelt E, Chen T, Wang D, Hope W, Boyer-Chammard T, Loyse A, Molloy SF, Youssouf N, Lortholary O, Lalloo DG, Jaffar S, Harrison TS, Ambition Study G. 2022. Single-Dose Liposomal Amphotericin B Treatment for Cryptococcal Meningitis. N Engl J Med 386:1109-1120.

bioRxiv preprint doi: https://doi.org/10.1101/2023.04.10.536237; this version posted April 12, 2023. The copyright holder for this preprint (which was not certified by peer review) is the author/funder, who has granted bioRxiv a license to display the preprint in perpetuity. It is made available under aCC-BY-ND 4.0 International license.

11. Valero G, Graybill JR. 1995. Successful treatment of cryptococcal meningitis with amphotericin B colloidal dispersion: report of four cases. Antimicrob Agents Chemother 39:2588-90.
12. Ngan NTT, Thanh Hoang Le N, Vi Vi NN, Van NTT, Mai NTH, Van Anh D, Trieu PH, Lan NPH, Phu NH, Chau NVV, Lalloo DG, Hope W, Beardsley J, White NJ, Geskus R, Thwaites GE, Krysan D, Tai LTH, Kestelyn E, Binh TQ, Hung LQ, Tung NLN, Day JN. 2021. An open label randomized controlled trial of tamoxifen combined with amphotericin B and fluconazole for cryptococcal meningitis. Elife 10.
13. Valenza M, Facchinetti R, Steardo L, Scuderi C. 2022. Palmitoylethanolamide and White Matter Lesions: Evidence for Therapeutic Implications. Biomolecules 12.
14. Zhou G, Fu X, Wang L, Cao Y, Zhuang J, Hu J, Li Y, Xu C, Gao S, Shao A, Wang L. 2022. Palmitoylethanolamide ameliorates neuroinflammation via modulating PPAR-alpha to promote the functional outcome after intracerebral hemorrhage. Neurosci Lett 781:136648.
15. D'Agostino G, La Rana G, Russo R, Sasso O, Iacono A, Esposito E, Mattace Raso G, Cuzzocrea S, Loverme J, Piomelli D, Meli R, Calignano A. 2009. Central administration of palmitoylethanolamide reduces hyperalgesia in mice via inhibition of NF-kappaB nuclear signalling in dorsal root ganglia. Eur J Pharmacol 613:54-9.
16. Lama A, Pirozzi C, Severi I, Morgese MG, Senzacqua M, Annunziata C, Comella F, Del Piano F, Schiavone S, Petrosino S, Mollica MP, Diano S, Trabace L, Calignano A, Giordano A, Mattace Raso G, Meli R. 2022. Palmitoylethanolamide dampens neuroinflammation and anxiety-like behavior in obese mice. Brain Behav Immun 102:110-123.
17. Orefice NS, Alhouayek M, Carotenuto A, Montella S, Barbato F, Comelli A, Calignano A, Muccioli GG, Orefice G. 2016. Oral Palmitoylethanolamide Treatment Is Associated with Reduced Cutaneous Adverse Effects of Interferon-beta1a and Circulating Proinflammatory Cytokines in Relapsing-Remitting Multiple Sclerosis. Neurotherapeutics 13:428-38.
18. Esposito E, Impellizzeri D, Mazzon E, Paterniti I, Cuzzocrea S. 2012. Neuroprotective activities of palmitoylethanolamide in an animal model of Parkinson's disease. PLoS One 7:e41880.

bioRxiv preprint doi: https://doi.org/10.1101/2023.04.10.536237; this version posted April 12, 2023. The copyright holder for this preprint (which was not certified by peer review) is the author/funder, who has granted bioRxiv a license to display the preprint in perpetuity. It is made available under aCC-BY-ND 4.0 International license.

19. Facchinetti R, Valenza M, Bronzuoli MR, Menegoni G, Ratano P, Steardo L, Campolongo P, Scuderi C. 2020. Looking for a Treatment for the Early Stage of Alzheimer's Disease: Preclinical Evidence with Co-Ultramicronized Palmitoylethanolamide and Luteolin. Int J Mol Sci 21.

20. Scuderi C, Valenza M, Stecca C, Esposito G, Carratu MR, Steardo L. 2012. Palmitoylethanolamide exerts neuroprotective effects in mixed neuroglial cultures and organotypic hippocampal slices via peroxisome proliferator-activated receptor-alpha. J Neuroinflammation 9:49.

21. Redlich S, Ribes S, Schutze S, Nau R. 2014. Palmitoylethanolamide stimulates phagocytosis of Escherichia coli K1 by macrophages and increases the resistance of mice against infections. J Neuroinflammation 11:108.

22. Beggiato S, Tomasini MC, Ferraro L. 2019. Palmitoylethanolamide (PEA) as a Potential Therapeutic Agent in Alzheimer's Disease. Front Pharmacol 10:821.

23. Kahlich R, Klima J, Cihla F, Frankova V, Masek K, Rosicky M, Matousek F, Bruthans J. 1979. Studies on prophylactic efficacy of N-2-hydroxyethyl palmitamide (Impulsin) in acute respiratory infections. Serologically controlled field trials. J Hyg Epidemiol Microbiol Immunol 23:11-24.

24. Keppel Hesselink JM, de Boer T, Witkamp RF. 2013. Palmitoylethanolamide: A Natural Body-Own Anti-Inflammatory Agent, Effective and Safe against Influenza and Common Cold. Int J Inflam 2013:151028.

25. Hamed MF, Enriquez V, Munzen ME, Charles-Nino CL, Mihu MR, Khoshbouei H, Alvina K, Martinez LR. 2023. Clinical and pathological characterization of Central Nervous System cryptococcosis in an experimental mouse model of stereotaxic intracerebral infection. PLoS Negl Trop Dis 17:e0011068.

26. Lee SC, Dickson DW, Casadevall A. 1996. Pathology of cryptococcal meningoencephalitis: analysis of 27 patients with pathogenetic implications. Hum Pathol 27:839-47.

27. Tien RD, Chu PK, Hesselink JR, Duberg A, Wiley C. 1991. Intracranial cryptococcosis in immunocompromised patients: CT and MR findings in 29 cases. AJNR Am J Neuroradiol 12:283-9.

bioRxiv preprint doi: https://doi.org/10.1101/2023.04.10.536237; this version posted April 12, 2023. The copyright holder for this preprint (which was not certified by peer review) is the author/funder, who has granted bioRxiv a license to display the preprint in perpetuity. It is made available under aCC-BY-ND 4.0 International license.

631 28. Hamed MF, Araujo GRS, Munzen ME, Reguera-Gomez M, Epstein C, Lee HH, Frases S,
632 Martinez LR. 2023. Phospholipase B Is Critical for Cryptococcus neoformans Survival in
633 the Central Nervous System. mBio doi:10.1128/mbio.02640-22:e0264022.
634 29. Fernandes KE, Brockway A, Haverkamp M, Cuomo CA, van Ogtrop F, Perfect JR,
635 Carter DA. 2018. Phenotypic Variability Correlates with Clinical Outcome in
636 Cryptococcus Isolates Obtained from Botswanan HIV/AIDS Patients. mBio 9.
637 30. Zaragoza O, Chrisman CJ, Castelli MV, Frases S, Cuenca-Estrella M, Rodriguez-Tudela
638 JL, Casadevall A. 2008. Capsule enlargement in Cryptococcus neoformans confers
639 resistance to oxidative stress suggesting a mechanism for intracellular survival. Cell
640 Microbiol 10:2043-57.
641 31. Ribes S, Ebert S, Czesnik D, Regen T, Zeug A, Bukowski S, Mildner A, Eiffert H,
642 Hanisch UK, Hammerschmidt S, Nau R. 2009. Toll-like receptor prestimulation increases
643 phagocytosis of Escherichia coli DH5alpha and Escherichia coli K1 strains by murine
644 microglial cells. Infect Immun 77:557-64.
645 32. Zhou Q, Gault RA, Kozel TR, Murphy WJ. 2007. Protection from direct cerebral
646 cryptococcus infection by interferon-gamma-dependent activation of microglial cells. J
647 Immunol 178:5753-61.
648 33. Nau R, Ribes S, Djukic M, Eiffert H. 2014. Strategies to increase the activity of microglia
649 as efficient protectors of the brain against infections. Front Cell Neurosci 8:138.
650 34. Coburn AF, Trulson MF, Moore LV. 1954. [Further study of the effect of the
651 administration of egg yolk on susceptibility of children to rheumatic infection]. Minerva
652 Med 45:1534-6.
653 35. Mesa-Arango AC, Trevijano-Contador N, Roman E, Sanchez-Fresneda R, Casas C,
654 Herrero E, Arguelles JC, Pla J, Cuenca-Estrella M, Zaragoza O. 2014. The production of
655 reactive oxygen species is a universal action mechanism of Amphotericin B against
656 pathogenic yeasts and contributes to the fungicidal effect of this drug. Antimicrob Agents
657 Chemother 58:6627-38.
658 36. Chen SF, Lu CH, Lui CC, Huang CR, Chuang YC, Tan TY, Tsai NW, Chang CC, Tsai
659 WC, Chang WN. 2011. Acute/subacute cerebral infarction (ASCI) in HIV-negative
660 adults with cryptococcal meningoencephalitis (CM): a MRI-based follow-up study and a
661 clinical comparison to HIV-negative CM adults without ASCI. BMC Neurol 11:12.

bioRxiv preprint doi: https://doi.org/10.1101/2023.04.10.536237; this version posted April 12, 2023. The copyright holder for this preprint (which was not certified by peer review) is the author/funder, who has granted bioRxiv a license to display the preprint in perpetuity. It is made available under aCC-BY-ND 4.0 International license.

662 37. Shimoda Y, Ohtomo S, Arai H, Ohtoh T, Tominaga T. 2017. Subarachnoid small vein
663 occlusion due to inflammatory fibrosis-a possible mechanism for cerebellar infarction in
664 cryptococcal meningoencephalitis: a case report. BMC Neurol 17:157.
665 38. Lee HH, Del Pozzo J, Salamanca SA, Hernandez H, Martinez LR. 2019. Reduced
666 phagocytosis and killing of Cryptococcus neoformans biofilm-derived cells by J774.16
667 macrophages is associated with fungal capsular production and surface modification.
668 Fungal Genet Biol 132:103258.
669 39. Yauch LE, Lam JS, Levitz SM. 2006. Direct inhibition of T-cell responses by the
670 Cryptococcus capsular polysaccharide glucuronoxylomannan. PLoS Pathog 2:e120.
671 40. Zaragoza O, Mihu C, Casadevall A, Nosanchuk JD. 2005. Effect of amphotericin B on
672 capsule and cell size in Cryptococcus neoformans during murine infection. Antimicrob
673 Agents Chemother 49:4358-61.
674 41. Stein JM, Burdon PJ. 1960. Cryptococcus neoformans infection of the central nervous
675 system: a case treated by amphotericin B, with postmortem examination. Ann Intern Med
676 52:445-53.
677 42. Wolf SA, Boddeke HW, Kettenmann H. 2017. Microglia in Physiology and Disease.
678 Annu Rev Physiol 79:619-643.
679 43. Lee SC, Kress Y, Zhao ML, Dickson DW, Casadevall A. 1995. Cryptococcus
680 neoformans survive and replicate in human microglia. Lab Invest 73:871-9.
681 44. Martini AC, Helman AM, McCarty KL, Lott IT, Doran E, Schmitt FA, Head E. 2020.
682 Distribution of microglial phenotypes as a function of age and Alzheimer's disease
683 neuropathology in the brains of people with Down syndrome. Alzheimers Dement (Amst)
684 12:e12113.
685 45. Ziebell JM, Taylor SE, Cao T, Harrison JL, Lifshitz J. 2012. Rod microglia: elongation,
686 alignment, and coupling to form trains across the somatosensory cortex after
687 experimental diffuse brain injury. J Neuroinflammation 9:247.
688 46. Bachstetter AD, Van Eldik LJ, Schmitt FA, Neltner JH, Ighodaro ET, Webster SJ, Patel
689 E, Abner EL, Kryscio RJ, Nelson PT. 2015. Disease-related microglia heterogeneity in
690 the hippocampus of Alzheimer's disease, dementia with Lewy bodies, and hippocampal
691 sclerosis of aging. Acta Neuropathol Commun 3:32.

bioRxiv preprint doi: https://doi.org/10.1101/2023.04.10.536237; this version posted April 12, 2023. The copyright holder for this preprint (which was not certified by peer review) is the author/funder, who has granted bioRxiv a license to display the preprint in perpetuity. It is made available under aCC-BY-ND 4.0 International license.

692 47. Streit WJ, Xue QS, Tischer J, Bechmann I. 2014. Microglial pathology. Acta
693 Neuropathol Commun 2:142.
694 48. Ohm DT, Fought AJ, Martersteck A, Coventry C, Sridhar J, Gefen T, Weintraub S, Bigio
695 E, Mesulam MM, Rogalski E, Geula C. 2021. Accumulation of neurofibrillary tangles
696 and activated microglia is associated with lower neuron densities in the aphasic variant of
697 Alzheimer's disease. Brain Pathol 31:189-204.
698 49. Wang C, Zong S, Cui X, Wang X, Wu S, Wang L, Liu Y, Lu Z. 2023. The effects of
699 microglia-associated neuroinflammation on Alzheimer's disease. Front Immunol
700 14:1117172.
701 50. Standaert DG, Harms AS, Childers GM, Webster JM. 2023. Disease mechanisms as
702 subtypes: Inflammation in Parkinson disease and related disorders. Handb Clin Neurol
703 193:95-106.
704 51. Peng L, Hu G, Yao Q, Wu J, He Z, Law BY, Hu G, Zhou X, Du J, Wu A, Yu L. 2022.
705 Microglia autophagy in ischemic stroke: A double-edged sword. Front Immunol
706 13:1013311.
707 52. Auge E, Bechmann I, Llor N, Vilaplana J, Krueger M, Pelegri C. 2019. Corpora
708 amylacea in human hippocampal brain tissue are intracellular bodies that exhibit a
709 homogeneous distribution of neo-epitopes. Sci Rep 9:2063.
710 53. Streit WJ, Braak H, Xue QS, Bechmann I. 2009. Dystrophic (senescent) rather than
711 activated microglial cells are associated with tau pathology and likely precede
712 neurodegeneration in Alzheimer's disease. Acta Neuropathol 118:475-85.
713 54. Kashef Hamadani BH, Franco-Paredes C, McCollister B, Shapiro L, Beckham JD,
714 Henao-Martinez AF. 2018. Cryptococcosis and cryptococcal meningitis: New predictors
715 and clinical outcomes at a United States academic medical centre. Mycoses 61:314-320.
716 55. Person AK, Ramirez BC, Kim A, Veloso V, Maruri F, Wandeler G, Fox M, Moore R,
717 Gill MJ, Imran D, Van Nguyen K, Nalitya E, Muyindike W, Shepherd BE, McGowan
718 CC. 2023. Cryptococcal Meningitis and Clinical Outcomes in Persons with HIV: A
719 Global View. Clin Infect Dis doi:10.1093/cid/ciad076.
720 56. Wiederhold NP, Kovanda L, Najvar LK, Bocanegra R, Olivo M, Kirkpatrick WR,
721 Patterson TF. 2016. Isavuconazole Is Effective for the Treatment of Experimental
722 Cryptococcal Meningitis. Antimicrob Agents Chemother 60:5600-3.

bioRxiv preprint doi: https://doi.org/10.1101/2023.04.10.536237; this version posted April 12, 2023. The copyright holder for this preprint (which was not certified by peer review) is the author/funder, who has granted bioRxiv a license to display the preprint in perpetuity. It is made available under aCC-BY-ND 4.0 International license.

723 57. Wiederhold NP, Najvar LK, Bocanegra R, Kirkpatrick WR, Sorrell TC, Patterson TF.
724 2013. Limited activity of miltefosine in murine models of cryptococcal
725 meningoencephalitis and disseminated cryptococcosis. Antimicrob Agents Chemother
726 57:745-50.
727

bioRxiv preprint doi: https://doi.org/10.1101/2023.04.10.536237; this version posted April 12, 2023. The copyright holder for this preprint (which was not certified by peer review) is the author/funder, who has granted bioRxiv a license to display the preprint in perpetuity. It is made available under aCC-BY-ND 4.0 International license.

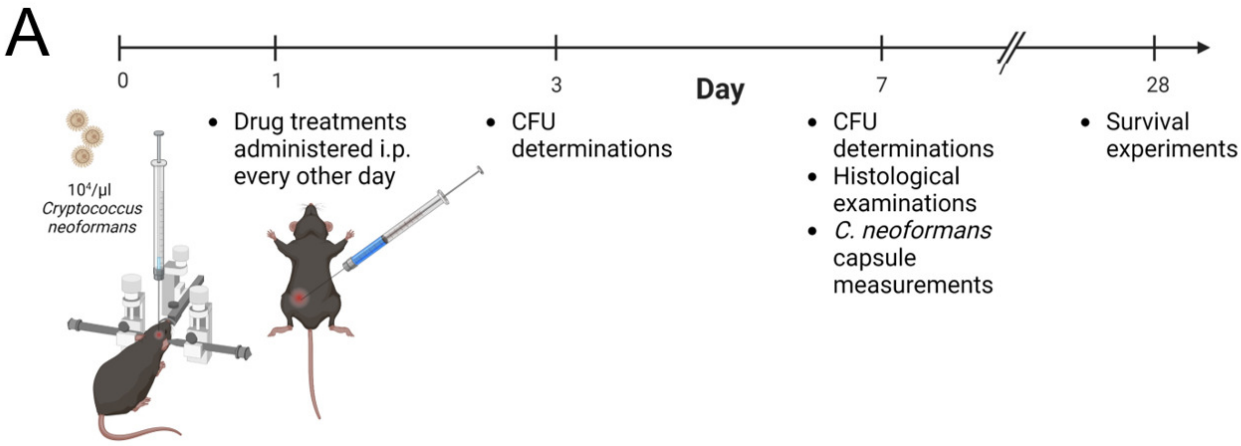

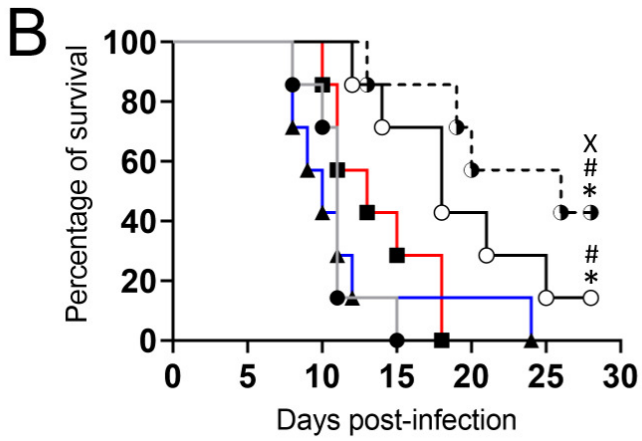

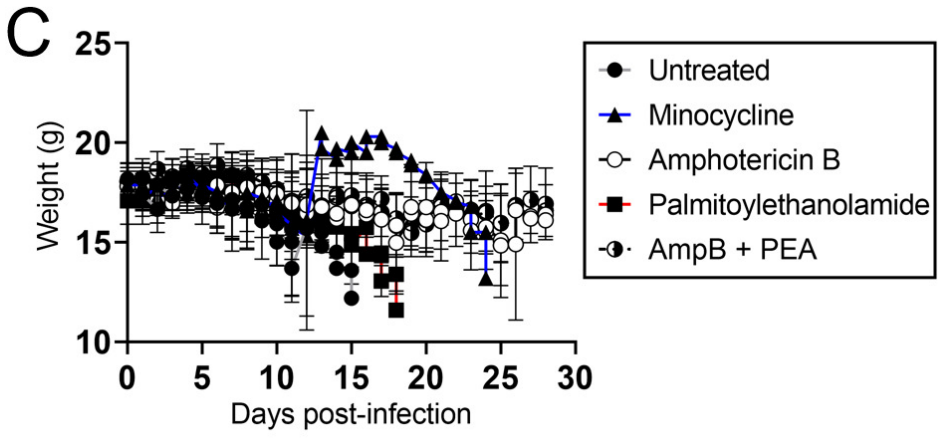

bioRxiv preprint doi: https://doi.org/10.1101/2023.04.10.536237; this version posted April 12, 2023. The copyright holder for this preprint (which was not certified by peer review) is the author/funder, who has granted bioRxiv a license to display the preprint in perpetuity. It is made available under aCC-BY-ND 4.0 International license.

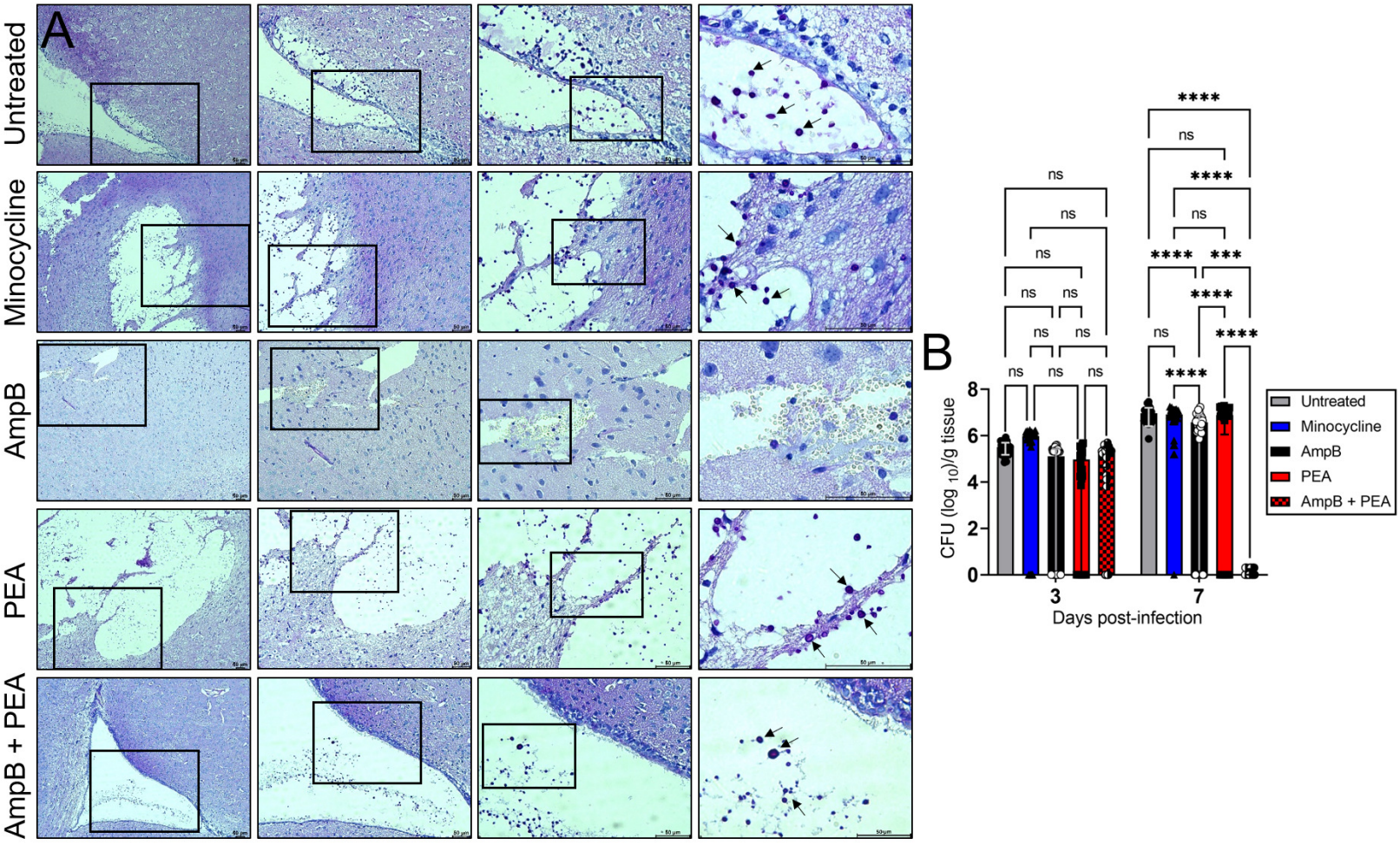

bioRxiv preprint doi: https://doi.org/10.1101/2023.04.10.536237; this version posted April 12, 2023. The copyright holder for this preprint (which was not certified by peer review) is the author/funder, who has granted bioRxiv a license to display the preprint in perpetuity. It is made available under aCC-BY-ND 4.0 International license.

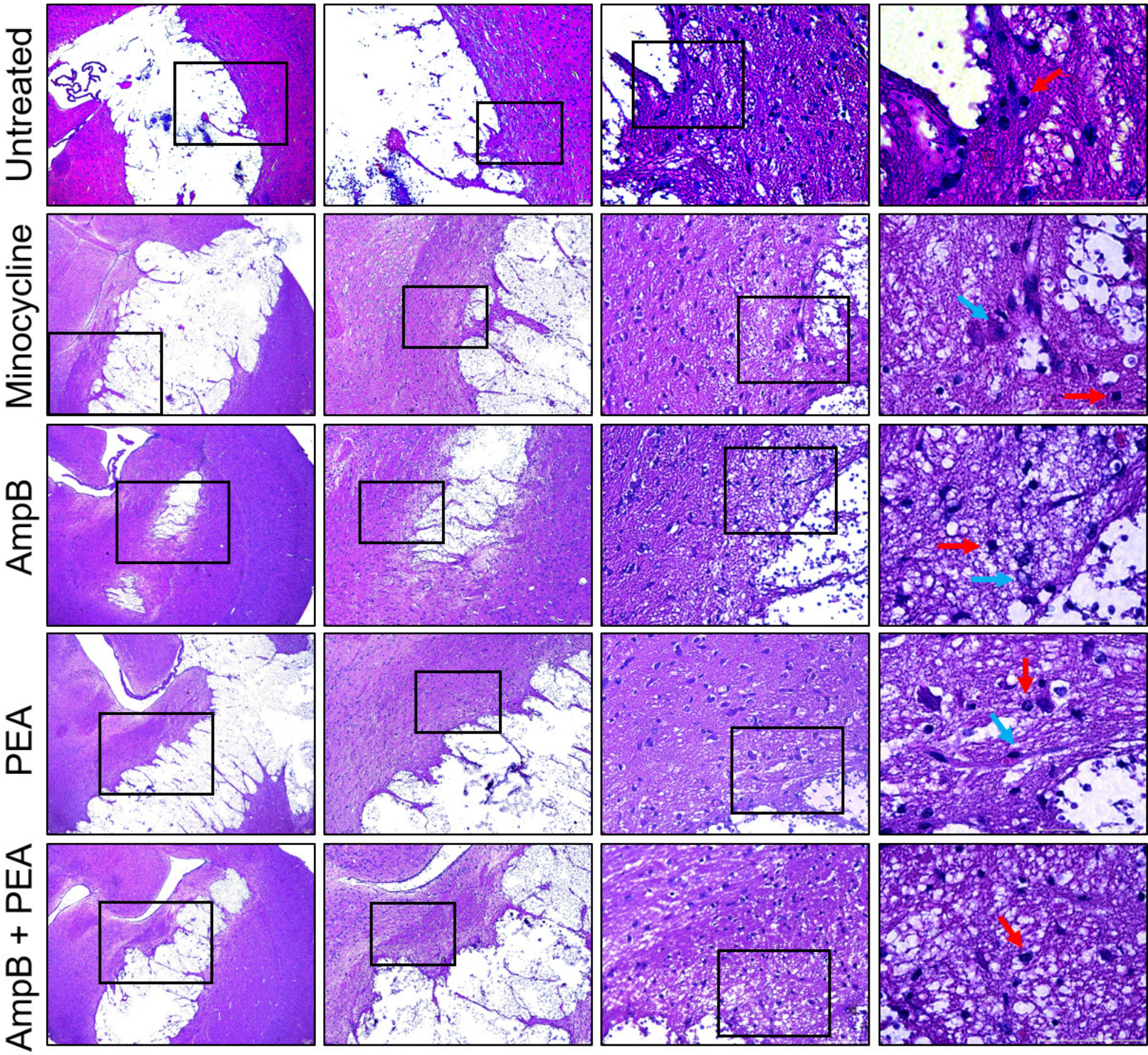

bioRxiv preprint doi: https://doi.org/10.1101/2023.04.10.536237; this version posted April 12, 2023. The copyright holder for this preprint (which was not certified by peer review) is the author/funder, who has granted bioRxiv a license to display the preprint in perpetuity. It is made available under aCC-BY-ND 4.0 International license.

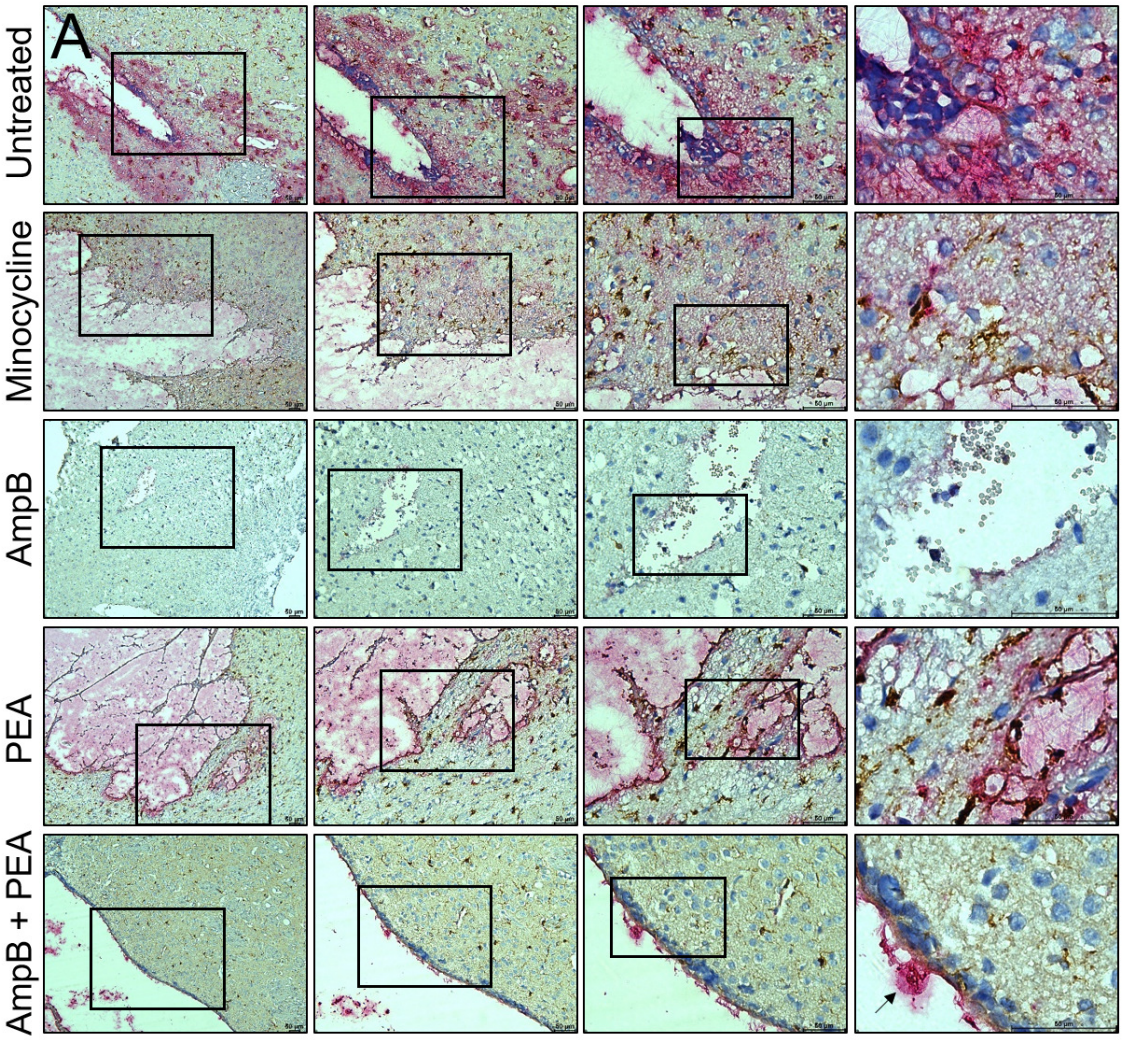

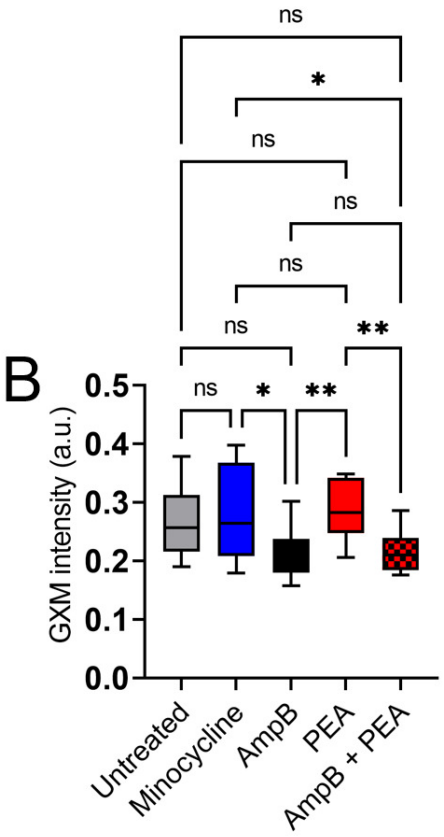

bioRxiv preprint doi: https://doi.org/10.1101/2023.04.10.536237; this version posted April 12, 2023. The copyright holder for this preprint (which was not certified by peer review) is the author/funder, who has granted bioRxiv a license to display the preprint in perpetuity. It is made available under aCC-BY-ND 4.0 International license.

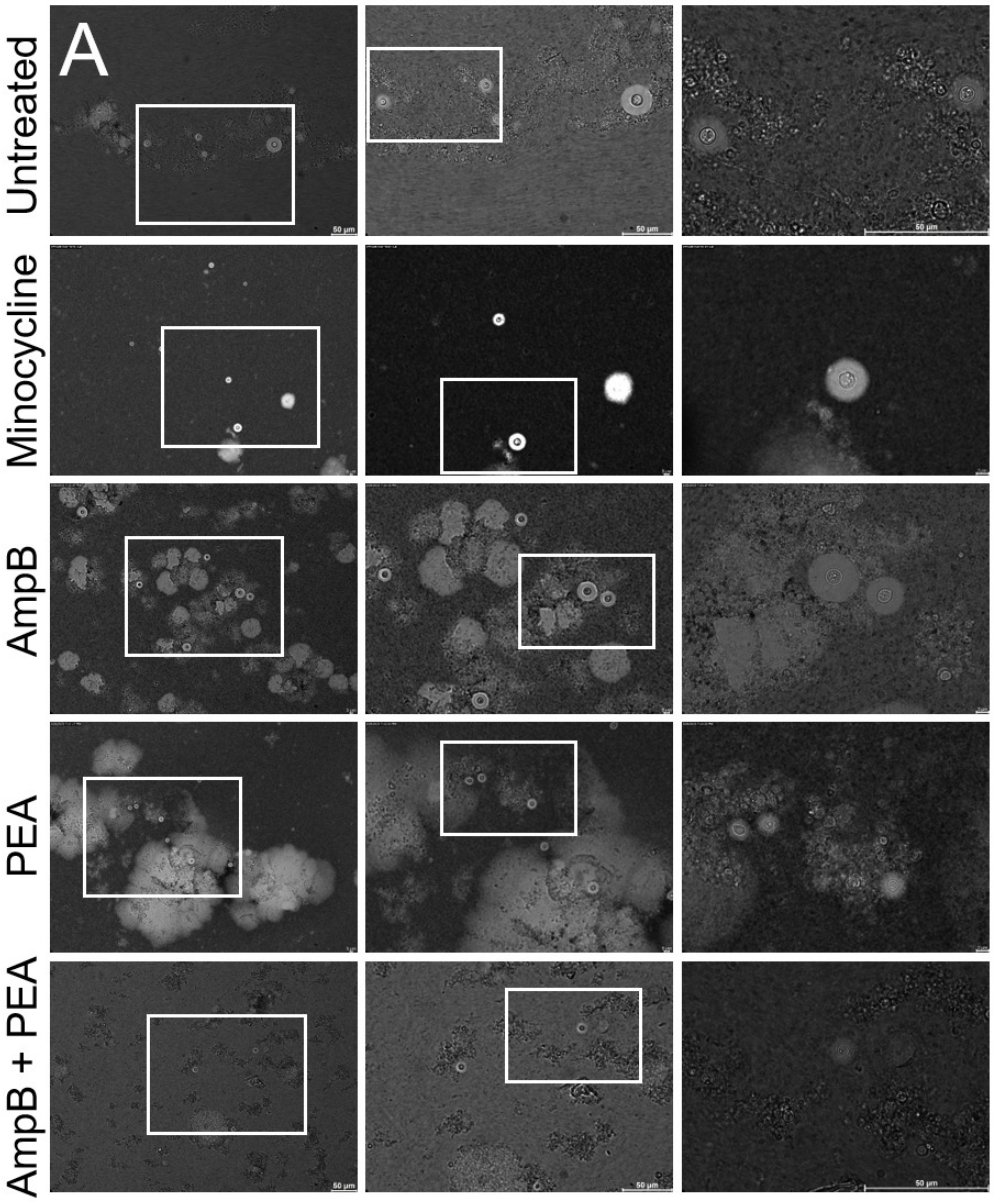

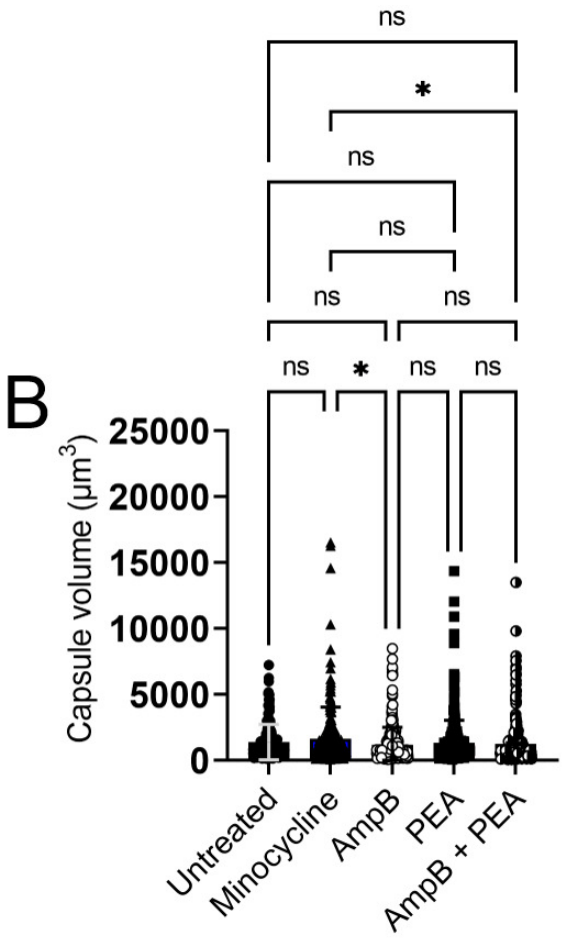

bioRxiv preprint doi: https://doi.org/10.1101/2023.04.10.536237; this version posted April 12, 2023. The copyright holder for this preprint (which was not certified by peer review) is the author/funder, who has granted bioRxiv a license to display the preprint in perpetuity. It is made available under aCC-BY-ND 4.0 International license.

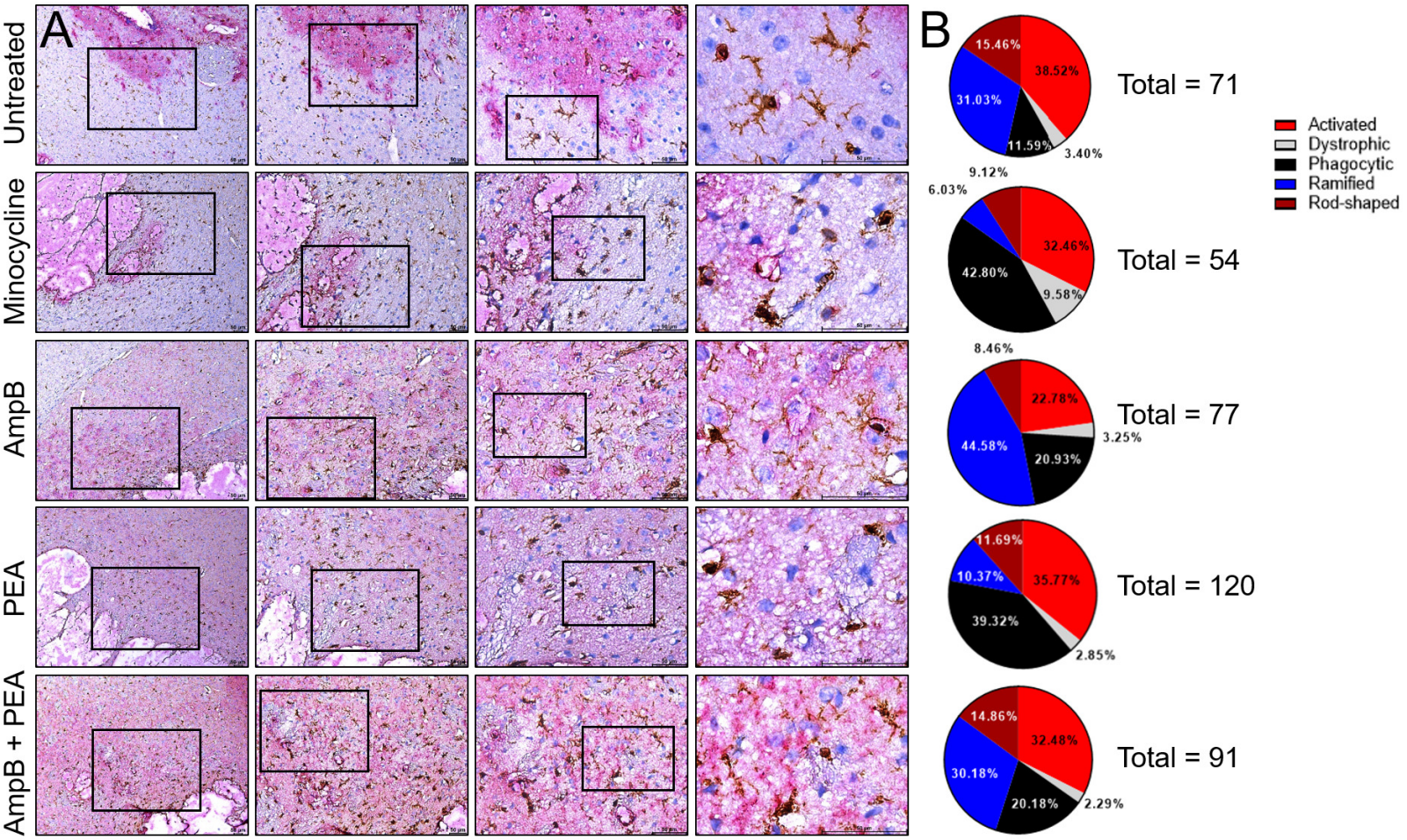

bioRxiv preprint doi: https://doi.org/10.1101/2023.04.10.536237; this version posted April 12, 2023. The copyright holder for this preprint (which was not certified by peer review) is the author/funder, who has granted bioRxiv a license to display the preprint in perpetuity. It is made available under aCC-BY-ND 4.0 International license.